Electrocatalysis

Deutsche Ausgabe: DOI: 10.1002/ange.201604654
Internationale Ausgabe: DOI: 10.1002/anie.201604654

Selective and Efficient Reduction of Carbon Dioxide to Carbon Monoxide on Oxide-Derived Nanostructured Silver Electrocatalysts

*Ming Ma, Bartek J. Trześniewski, Jie Xie, and Wilson A. Smith**

Abstract: *In this work, the selective electrocatalytic reduction of carbon dioxide to carbon monoxide on oxide-derived silver electrocatalysts is presented. By a simple synthesis technique, the overall high faradaic efficiency for CO production on the oxide-derived Ag was shifted by more than 400 mV towards a lower overpotential compared to that of untreated Ag. Notably, the Ag resulting from Ag oxide is capable of electrochemically reducing CO_2 to CO with approximately 80 % catalytic selectivity at a moderate overpotential of 0.49 V, which is much higher than that (ca. 4 %) of untreated Ag under identical conditions. Electrokinetic studies show that the improved catalytic activity is ascribed to the enhanced stabilization of $COOH^{\cdot}$ intermediate. Furthermore, highly nanostructured Ag is likely able to create a high local pH near the catalyst surface, which may also facilitate the catalytic activity for the reduction of CO_2 with suppressed H_2 evolution.*

The electrochemical conversion of CO_2 into carbon-based fuels is an attractive strategy for utilizing CO_2 captured at large emission sources.[1–5] In order to close the anthropogenic carbon cycle, the electrocatalytic reduction of CO_2 to fuels should be powered by a renewable electricity source.[6] For achieving this goal, the essential step is to develop a cheap, stable, and efficient catalyst with high selectivity for a desired product. Over the past few decades, several catalyst materials with the capability of reducing CO_2 electrochemically in CO_2 saturated-aqueous solutions have been identified.[3,7–18] It has been demonstrated that polycrystalline Au is capable of reducing CO_2 to CO with a high faradaic efficiency (FE) of about 87 % at −0.74 vs. reversible hydrogen electrode (RHE).[5] While Au is currently the most efficient electrocatalytic surface for CO_2 reduction to CO, the low abundance and high cost of Au may prevent its large-scale applications. To find a cost-effective and stable catalyst with high selectivity and efficiency remains a challenge for achieving practical utilization of CO_2 reduction to CO.

Metallic Ag has attracted considerable attention due to its significantly lower cost compared to Au and high selectivity for the conversion of CO_2 to CO.[7,11] However, the high overpotential (> 0.9 V) on Ag catalysts is required for driving the electrocatalytic reduction of CO_2 efficiently and selectively with suppressed H_2O reduction.[5] The large overpotential required for the reduction of CO_2 is attributed to the hindrance for the initial electron transfer to a CO_2 molecule.[2,19–21] Lu et al.[19] reported that a nanoporous Ag catalyst with a fast initial electron transfer prepared by the de-alloying of an Ag-Al prescursor is capable of reducing CO_2 electrochemically to CO efficiently and selectively at reduced overpotential. Recently, Kanan et al.[21,22] discovered that oxide-derived Cu and Au nanoparticle films exhibit a dramatically improved selectivity for the reduction of CO_2 to CO at low overpotential and high resistance to catalytic deactivation compared to polycrystalline metals.

This study is the first exploration of the catalytic activity of the electrochemical reduction of CO_2 on oxide-derived nanostructured Ag catalysts (OD-Ag). Here we demonstrate that a nanostructured Ag electrode resulting from silver oxide is capable of electrochemically reducing CO_2 to CO with high selectivity at much lower overpotential compared to that of the polycrystalline Ag, and the increased catalytic activity is linked to the improved stabilization of the $COOH^{\cdot}$ intermediate.

The thermal oxidation of Ag foils is prohibited because the decomposition of silver oxide becomes significant at temperatures above 200 °C.[23] Here, we used a simple and scalable electrochemical method for oxidizing Ag electrodes. Potential anodization in alkaline solutions was an effective and simple method for the formation of Ag oxide on Ag electrodes.[24–28] Here, an electrode made of a polycrystalline Ag foil was immersed in 0.2 M NaOH solutions in a two-compartment cell with a Pt counter electrode and an Ag/AgCl reference electrode (cyclic voltammetry of Ag in 0.2 M NaOH is shown in Figure S1 in the Supporting Information). The two-compartment cell was separated by a Nafion-115 proton exchange membrane to avoid Pt deposition on Ag electrodes during the electrochemical synthesis. A symmetric 50 Hz square-wave pulsed potential was applied on Ag electrodes to synthesize Ag oxide layers. We found that the fabricated Ag oxide layers exhibit a porous structure, as shown in Figure S2. The resulting Ag oxide electrodes were directly used in the electrochemical reduction of CO_2, and were electrochemically reduced to metallic Ag in the early stage of electrolysis.

Figure 1 a,b show scanning electron microscope (SEM) images of electrodes resulting from Ag oxide after the

[*] M. Ma, B. J. Trześniewski, Dr. W. A. Smith
Materials for Energy Conversion and Storage (MECS)
Department of Chemical Engineering, Delft University of Technology
P.O. Box 5045, 2600 GA Delft (The Netherlands)
E-mail: W.Smith@tudelft.nl
M. Ma
State Key Laboratory of Heavy Oil Processing
China University of Petroleum
Qingdao 266580, Shandong (P.R. China)
J. Xie
Department of Chemical Engineering and Chemistry
Eindhoven University of Technology
5600 MB Eindhoven (The Netherlands)

Supporting information for this article can be found under: http://dx.doi.org/10.1002/anie.201604654.

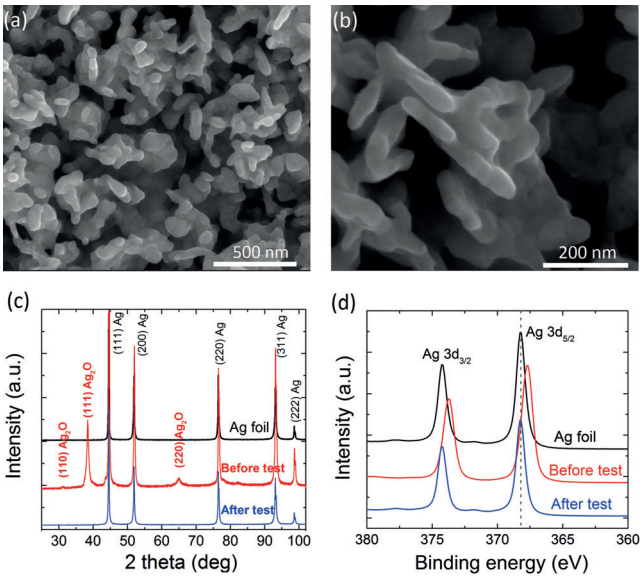

Figure 1. a,b) SEM images of oxide-derived Ag. c) XRD patterns and d) XPS spectrum of the polycrystalline Ag electrode (black line) and Ag oxide electrode before (red line) and after (blue line) CO_2 reduction electrolysis, respectively.

electrocatalytic reduction of CO_2 in CO_2-saturated electrolytes. The SEM images indicate that a porous-like nanostructured Ag surface was formed as a result of the reduction of Ag oxide after electrolysis. The X-ray diffraction (XRD) pattern in Figure 1 c confirms the presence of Ag_2O on Ag foil synthesized by anodization in alkaline solutions. After CO_2 reduction electrolysis, XRD pattern shows only Ag peaks with no more indication of any remaining Ag oxide. In addition, the Ag foil fabricated by anodization turned a black color (Figure S3), which is also indicative of the formation of Ag oxide, and the sample had no remaining black color after CO_2 reduction electrolysis.

To further confirm the composition of the samples before and after electrolysis, X-ray photoelectron spectroscopy (XPS) measurements were performed. The Ag $3d_{5/2}$ peak at 368.2 eV was observed for polycrystalline Ag in Figure 1 d. For the synthesized Ag oxide, the Ag $3d_{5/2}$ peak shifted to the binding energy of 367.7 eV, which corresponds to the Ag_2O formation according to the Ag $3d_{5/2}$ peak analysis for Ag and Ag oxide in previous work.[29] After electrolysis, the Ag $3d_{5/2}$ peak shifted back to 368.2 eV, implying the surface was metallic Ag without any Ag oxide.[29] The Ag 3d XPS spectrum analysis is consistent with the results of the XRD patterns, indicating the electroreduction of Ag_2O to metallic Ag was complete within the detection limit of these characterization techniques.

The electrocatalytic reduction of CO_2 on OD-Ag and polycrystalline Ag were performed in CO_2-saturated 0.1 M $KHCO_3$ (99.95 %) electrolyte (pH 6.83) at ambient temperature and pressure. In the initial period of electrolysis, OD-Ag electrodes were directly formed in situ by the electroreduction of the Ag oxide film formed on the Ag electrode. CO_2 reduction electrolysis experiments were performed in an electrochemical cell consisting of working and counter electrode compartments, separated by a Nafion-115 proton exchange membrane to prevent the oxidation of CO_2 reduction products. The cathodic compartment was continuously purged with CO_2 at a constant flow rate and vented directly into the gas-sampling loop of a gas chromatograph (GC) for the periodic quantification of the gas-phase products. Liquid products formed in the CO_2 reduction were detected by ^1H nuclear magnetic resonance (NMR) spectroscopy after completion of the electrolysis experiments.

The comparison of the CO_2 reduction activity of untreated polycrystalline Ag and OD-Ag is presented in Figure 2. The OD-Ag exhibited a high initial current density (j_{tot}) (Figure S4), which stems from the reduction of the Ag oxide layer in the initial period of electrolysis. Subsequently, the OD-Ag exhibited a j_{tot} of 1.15 mA cm^{-2} with CO faradaic efficiency of 89 % at −0.8 V vs. RHE, as shown in Figure 2 a. At a less negative potential of −0.7 V vs. RHE, a decreased FE of 82.4 % for CO formation was observed (Figure 2 b). Notably, the FE of 80 % for CO production was achieved at −0.6 V vs. RHE (Figure 2 c), corresponding to a modest overpotental (η_{CO}) of 0.49 V relative to the CO_2/CO equilibrium potential of −0.11 V vs. RHE. In contrast, the polycrystalline Ag electrodes experienced low j_{tot}, accompanying with very low FE for CO formation (22.4 %, 12 % and 4.1 % at −0.8 V, −0.7 V and −0.6 V vs. RHE, respectively).

To better understand the catalytic activity for CO_2 reduction, the FE for the major products of CO_2 reduction was plotted at various potentials for the polycrystalline Ag and the OD-Ag (Figure 3). As noted in Figure 3 a, the FE for

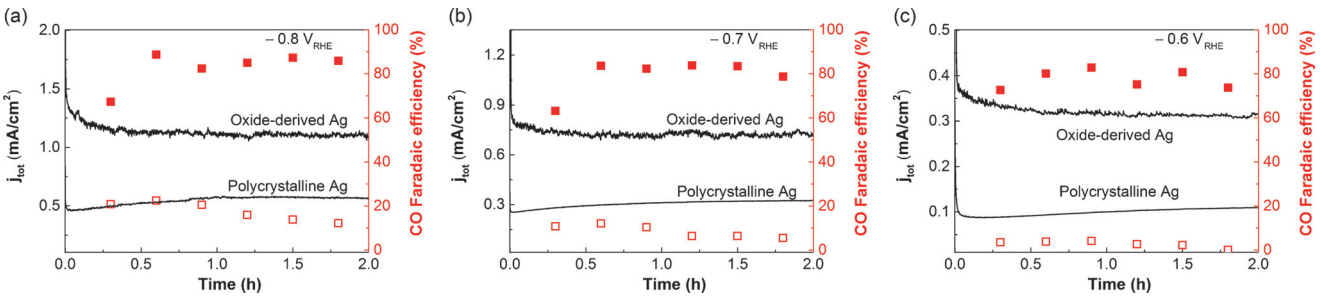

Figure 2. CO_2 reduction performance of untreated Ag and oxide-derived Ag. The total current density (left axis) and the CO faradaic efficiency (right axis) on untreated Ag and oxide-derived Ag (■ and □ represent CO faradaic efficiency on oxide-derived Ag and untreated Ag, respectively) at a) −0.8 V and b) −0.7 V, and c) −0.6 V versus RHE in CO_2-saturated 0.1 M $KHCO_3$ electrolytes.

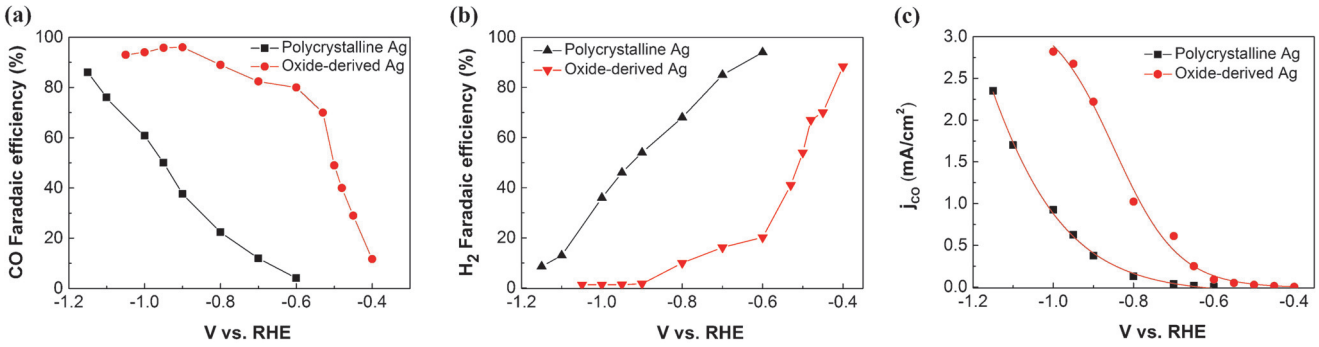

Figure 3. Comparison of the electrocatalytic activity of polycrystalline Ag and oxide-derived Ag. Faradaic efficiency for CO (a) and H_2 (b) on polycrystalline Ag and oxide-derived Ag at various potentials in CO_2-saturated 0.1 M $KHCO_3$ (pH 6.8). c) Current density for CO at various potentials.

the electrochemical reduction of CO_2 to CO on both the polycrystalline Ag and the OD-Ag gradually increased with enhancing overpotentials. The increase of the FE for CO corresponds to a decrease in the related FE for H_2 production (Figure 3b). In addition, a small amount of formate was only detected at high overpotentials (Figure S5). Interestingly, Figure 3a shows that the overall FE for CO on the OD-Ag was shifted by >400 mV toward the positive potential compared to that of untreated Ag (at a FE range for CO of more than 30%). In addition, the current density for CO production as a function of potentials in Figure 3c implies the onset potential for CO_2 reduction on OD-Ag was -0.4 V vs. RHE ($\eta_{CO} = 0.29$ V), which is a positive shift by about 200 mV compared to that (-0.6 V vs. RHE) of polycrystalline Ag. More importantly, for driving the electrocatalytic reduction of CO_2 to CO with a high FE of 80%, a potential of -0.6 V vs. RHE was required on OD-Ag, which is significantly reduced by 500 mV compared to that of untreated Ag (-1.1 V vs. RHE). These results indicate that OD-Ag acts as an efficient catalyst for the electrocatalytic reduction of CO_2 to CO with significantly suppressed H_2 evolution at decreased overpotentials.

To gain insight into the electrokinetic mechanism of CO_2 reduction on both catalysts, Tafel analysis was performed. Here, Tafel plots of the OD-Ag and the polycrystalline Ag (overpotential versus log of the partial current density for CO production) are shown in Figure 4. Hori has proposed that a two-electron transfer is involved in the electrochemical reduction of CO_2 to CO (Scheme 1).[11,30] In addition, most of the computational studies on reaction paths for CO_2 reduction are based on the computational hydrogen electrode (CHE) model, in which it is assumed that a proton-coupled electron transfer (PCET) takes place at every reaction step.[31–35] Thus, a COOH• is assumed to be formed by a PCET as the first CO_2 activation step in density functional theory (DFT) simulations.[31,33–35] However, in some experimental work, it is believed that the adsorbed $CO_2^{\bullet-}$ intermediate is formed on the active sites of the metal surface through a one-electron transfer to a CO_2 molecule, and then the COOH• intermediate is produced after accepting one proton.[19–22,36] Furthermore, it was reported that the first donation of a proton is from HCO_3^-.[19,21,35] Subsequently, the COOH• intermediate on the surface takes another electron and proton to form a CO and a H_2O molecule. It has been demonstrated that the initial electron transfer for CO_2 activation is the rate-determining step (RDS) for the overall process because the first electron transfer requires a much more negative potential compared to the following steps.[2,19–21]

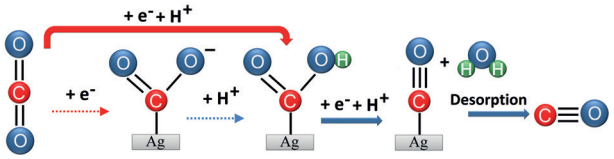

Scheme 1. Proposed reaction paths for electrocatalytic reduction of CO_2 to CO.

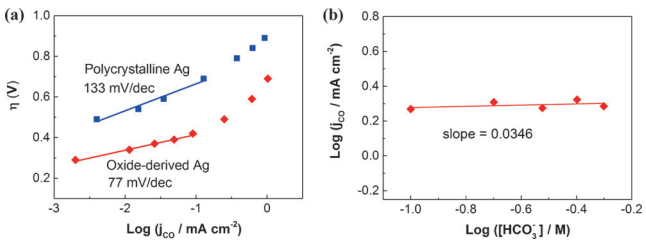

Figure 4. a) Tafel plots of the CO partial current density for polycrystalline Ag and oxide-derived Ag. b) Bicarbonate concentration at constant potential for oxide-derived Ag.

A Tafel slope of 133 mV dec^{-1} for polycrystalline Ag shown in Figure 4a corresponds to a transfer coefficient of 0.44 [Eq. (S2)]. This slope and the transfer coefficient are consistent with the fact that the rate-determining step is the initial electron transfer to CO_2.[11,19] In contrast, OD-Ag exhibited a low Tafel slope of 77 mV dec^{-1} at low overpotentials, which indicates a fast initial electron transfer to a CO_2 molecule according to previous studies.[7,19,21,22] Subsequently, we found a dramatic increases of the Tafel slope for OD-Ag at relatively high overpotentials, indicating the CO_2 electroreduction may reach a mass transport limitation on the porous-like nanostructured Ag.[35] Thus, while the mass transport in a nanostructured Ag catalyst is likely slower than in an untreated Ag (flat surface) at relatively high

overpotentials, OD-Ag can offer better stabilization for the COOH• intermediate than untreated Ag, thus decreasing the overpotential needed to drive CO_2 reduction to CO.

To further investigate the electrokinetics of CO_2 reduction on OD-Ag, electrolysis was performed at the HCO_3^- concentrations from 0.5 to 0.1 M. A plot of $\log(j_{CO})$ vs. $\log([HCO_3^-])$ in Figure 4b shows a zero-order dependence of HCO_3^- concentrations on CO_2 reduction activity, indicating that the donation of a proton from HCO_3^- is not a rate-determining step for CO_2 reduction.[19]

It was reported that the surface of nanostructured Ag catalysts can provide the low-coordinated surface Ag sites, which plays a significant role for stabilizing the COOH• intermediate through reducing the activation energy barrier of the initial electron transfer.[35] In addition, Kanan et al. proposed a grain boundary effect for OD-Cu[37] and OD-Au.[38] Here we propose a local pH effect to offer a new insight into the correlation of nanostructured Ag catalysts with the catalytic activity for CO_2 reduction. The pH rises locally at the electrode/electrolyte interface because of releasing OH^- in the cathodic reactions (Equation S (4–5)).[39] Thus, the pH close to the electrode (local pH) is higher than the bulk pH. To understand the local pH effect, CO_2 reduction was performed on flat Ag and OD-Ag in 0.1 M K_2HPO_4 and 0.1 M $KHCO_3$, respectively. The FE for CO on flat Ag was measured on flat Ag in 0.1 M $KClO_4$. $KClO_4$ does not have buffer ability, which results in a relatively high local pH at the electrode/electrolyte interface. We found that the FE for CO in CO_2-saturated 0.1 M $KClO_4$ was obviously higher than that of CO_2-saturated 0.1 M $KHCO_3$ (Figure 5a). These observations (the FE for CO on flat Ag: $KClO_4 > KHCO_3 > K_2HPO_4$) imply that the local pH may play an important role in the reduction of CO_2.

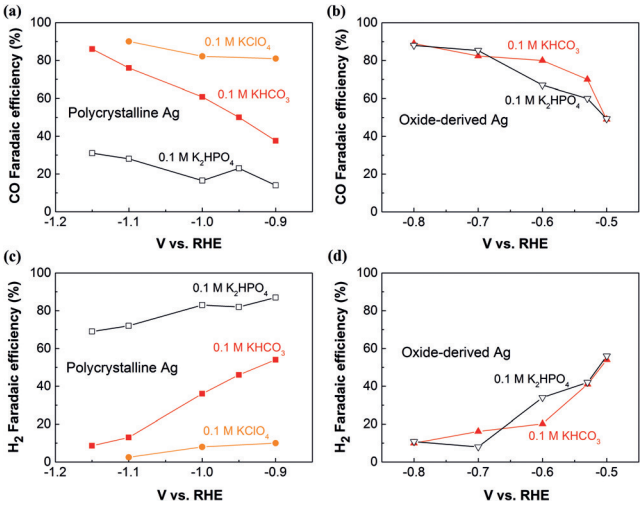

Figure 5. Faradaic efficiency for CO and H_2 on polycrystalline Ag (a,c) and oxide-derived Ag (b,d) at various potentials in CO_2-saturated 0.1 M K_2HPO_4 and CO_2-saturated 0.1 M $KHCO_3$, respectively. CO2 reduction on flat Ag was also performed in CO_2-saturated 0.1 M $KClO_4$.

significantly reduced (Figure 5a) with dramatically enhanced FE for H_2 (Figure 5c) in CO_2-saturated 0.1 M K_2HPO_4, which is consistent with the work of Hori on flat Cu (FE for H_2 is 72.4% and 10.9% in 0.1 M K_2HPO_4 and 0.1 M $KHCO_3$, respectively).[11] This observation is due to the fact that the buffer action of CO_2-saturated 0.1 M K_2HPO_4 can easily neutralize OH^- generated at the electrode surface, keeping local pH at relatively low value. The low pH value at the electrode/electrolyte interface favors H_2 evolution.[11] To further improve the local pH effect, CO_2 reduction was also

In contrast, we found that FE for CO on OD-Ag was almost equal in the two different electrolytes (Figure 5b) at various potentials. This observation may be partly attributed to that the limitation of the diffusion process in nanoporous Ag catalysts (Figure 1a,b) hinders the neutralization reaction for OH^- generated near the catalyst surface, resulting in a high local pH in 0.1 M K_2HPO_4. In addition, H_2 evolution is not favorable at the high pH value. Thus, the high local pH created in nanoporous Ag may contribute to the suppressed H_2 evolution (Figure 5d) with preferred CO_2 reduction (Figure 5b).

In summary, nanostructured Ag catalysts prepared by electrochemically reducing Ag_2O exhibited an enhanced catalytic activity for the reduction of CO_2, and the high selectivity for CO was shifted by more than 400 mV to a lower overpotential than that of untreated polycrystalline Ag. At a moderate overpotential of 0.49 V, the oxide-derived nanostructured Ag was able to reduce CO_2 to CO with about 80% faradaic efficiency, which is dramatically higher compared to that (ca. 4%) of untreated polycrystalline Ag at identical conditions. The dramatically improved catalytic activity and selectivity for CO_2 reduction to CO is likely correlated with the nanostructured surface, resulting in highly active sites for stabilizing COOH• intermediate. In addition, a high local pH generated within the porous-like nanostructured Ag catalysts may also play a role in the improved CO_2 reduction along with suppressed H_2 evolution. This study shows that a selective and cost-effective oxide-derived Ag catalyst can efficiently and selectively reduce CO_2 to CO. While the catalytic activity of this oxide-derived Ag catalyst is not as high as the recent oxide-derived Au, its cost is significantly lower, and thus this catalyst and synthetic approach may provide a more practical platform for large-scale CO_2 electroreduction.

Acknowledgements

This work is supported by CSC, and the NWO VENI grant awarded to Wilson A. Smith. The authors would like to thank Dr. Kristina Djanashvili for assistance in the 400 MHz NMR experiments. We also would like to thank Prof. Bernard Dam and Dr. David Vermaas for helpful discussions.

Keywords: carbon dioxide · conversion of carbon dioxide · electrocatalysis · heterogeneous catalysis · surface chemistry

How to cite: *Angew. Chem. Int. Ed.* **2016**, *55*, 9748–9752
Angew. Chem. **2016**, *128*, 9900–9904

[1] D. T. Whipple, P. J. A. Kenis, *J. Phys. Chem. Lett.* **2010**, *1*, 3451–3458.

[2] Y. Chen, M. W. Kanan, *J. Am. Chem. Soc.* **2012**, *134*, 1986 – 1989.
[3] J. Qiao, Y. Liu, F. Hong, J. Zhang, *J. Chem. Soc. Rev.* **2014**, *43*, 631 – 675.
[4] N. Kornienko, Y. Zhao, C. S. Kley, C. Zhu, D. Kim, S. Lin, C. J. Chang, O. M. Yaghi, P. Yang, *J. Am. Chem. Soc.* **2015**, *137*, 14129 – 14135.
[5] K. P. Kuhl, T. Hatsukade, E. R. Cave, D. N. Abram, J. Kibsgaard, T. F. Jaramillo, *J. Am. Chem. Soc.* **2014**, *136*, 14107 – 14113.
[6] M. Ma, K. Djanashvili, W. A. Smith, *Phys. Chem. Chem. Phys.* **2015**, *17*, 20861 – 20867.
[7] M. Gattrell, N. Gupta, A. Co, *J. Electroanal. Chem.* **2006**, *594*, 1 – 19.
[8] K. P. Kuhl, E. R. Cave, D. N. Abram, T. F. Jaramillo, *Energy Environ. Sci.* **2012**, *5*, 7050 – 7059.
[9] K. Manthiram, B. J. Beberwyck, A. P. Alivisatos, *J. Am. Chem. Soc.* **2014**, *136*, 13319 – 13325.
[10] Y. Hori, R. Takahashi, Y. Yoshinami, A. Murata, *J. Phys. Chem. B* **1997**, *101*, 7075 – 7081.
[11] Y. Hori in *Modern Aspects of Electrochemistry*, *Vol. 42* (Eds.: C. G. Vayenas, R. E. White, M. E. Gamboa-Aldeco), Springer, New York, **2008**, pp. 89 – 189.
[12] S. Zhang, P. Kang, S. Ubnoske, M. K. Brennaman, N. Song, R. L. House, J. T. Glass, T. J. Meyer, *J. Am. Chem. Soc.* **2014**, *136*, 7845 – 7848.
[13] J. Tamura, A. Ono, Y. Sugano, C. Huang, H. Nishizawa, S. Mikoshiba, *Phys. Chem. Chem. Phys.* **2015**, *17*, 26072 – 26078.
[14] D. A. Torelli, S. A. Francis, J. C. Crompton, A. Javier, J. R. Thompson, B. S. Brunschwig, M. P. Soriaga, N. S. Lewis, *ACS Catal.* **2016**, *6*, 2100 – 2104.
[15] M. Ma, K. Djanashvili, W. A. Smith, *Angew. Chem. Int. Ed.* **2016**, *55*, 6680 – 6684; *Angew. Chem.* **2016**, *128*, 6792 – 6796.
[16] S. Rasul, D. H. Anjum, A. Jedidi, Y. Minenkov, L. Cavallo, K. Takanabe, *Angew. Chem. Int. Ed.* **2015**, *54*, 2146 – 2150; *Angew. Chem.* **2015**, *127*, 2174 – 2178.
[17] A. Loiudice, P. Lobaccaro, E. A. Kamali, T. Thao, B. H. Huang, J. W. Ager, R. Buonsanti, *Angew. Chem. Int. Ed.* **2016**, *55*, 5789 – 5792; *Angew. Chem.* **2016**, *128*, 5883 – 5886.
[18] R. Kas, K. K. Hummadi, R. Kortlever, P. de Wit, A. Milbrat, M. W. J. Luiten-Olieman, N. E. Benes, M. T. M. Koper, G. Mul, *Nat. Commun.* **2016**, *7*, 10748.
[19] Q. Lu, J. Rosen, Y. Zhou, G. S. Hutchings, Y. C. Kimmel, J. G. Chen, F. Jiao, *Nat. Commun.* **2014**, *5*, 3242.
[20] Q. Lu, J. Rosen, F. Jiao, *ChemCatChem* **2015**, *7*, 38 – 47.
[21] Y. Chen, C. W. Li, M. W. Kanan, *J. Am. Chem. Soc.* **2012**, *134*, 19969 – 19972.
[22] C. W. Li, M. W. Kanan, *J. Am. Chem. Soc.* **2012**, *134*, 7231 – 7234.
[23] G. B. Hoflund, Z. F. Hazos, *Phys. Rev. B* **2000**, *62*, 11126 – 11133.
[24] T. P. Dirkse, *Electrochim. Acta* **1990**, *35*, 1445 – 1449.
[25] V. Maurice, L. Klein, H.-H. Strehblow, P. Marcus, *J. Phys. Chem. C* **2007**, *111*, 16351 – 16361.
[26] J. M. M. Droog, F. Huisman, *J. Electroanal. Chem. Interfacial Electrochem.* **1980**, *115*, 211 – 224.
[27] J. Gomez Becerra, R. C. Salvarezza, A. J. Arvia, *Electrochim. Acta* **1988**, *33*, 1431 – 1437.
[28] J. Ambrose, R. G. Barradas, *Electrochim. Acta* **1974**, *19*, 781 – 786.
[29] X.-Y. Gao, S.-Y. Wang, J. Li, Y.-X. Zheng, R.-J. Zhang, P. Zhou, Y.-M. Yang, L.-Y. Chen, *Thin Solid Films* **2004**, *455 – 456*, 438 – 442.
[30] Y. Hori, H. Wakebe, T. Tsukamoto, O. Koga, *Electrochim. Acta* **1994**, *39*, 1833 – 1839.
[31] R. Kortlever, J. Shen, K. J. P. Schouten, F. Calle-Vallejo, M. T. M. Koper, *J. Phys. Chem. Lett.* **2015**, *6*, 4073 – 4082.
[32] F. Calle-Vallejo, M. T. M. Koper, *Angew. Chem. Int. Ed.* **2013**, *52*, 7282 – 7285; *Angew. Chem.* **2013**, *125*, 7423 – 7426.
[33] A. A. Peterson, F. Abild-Pedersen, F. Studt, J. Rossmeisl, J. K. Nørskov, *Energy Environ. Sci.* **2010**, *3*, 1311.
[34] H. A. Hansen, J. B. Varley, A. A. Peterson, J. K. Nørskov, *J. Phys. Chem. Lett.* **2013**, *4*, 388 – 392.
[35] J. Rosen, G. S. Hutchings, Q. Lu, S. Rivera, Y. Zhou, D. G. Vlachos, F. Jiao, *ACS Catal.* **2015**, *5*, 4293 – 4299.
[36] C. H. Lee, M. W. Kanan, *ACS Catal.* **2015**, *5*, 465 – 469.
[37] C. W. Li, J. Ciston, M. W. Kanan, *Nature* **2014**, *508*, 504 – 507.
[38] X. Feng, K. Jiang, S. Fan, M. W. Kanan, *J. Am. Chem. Soc.* **2015**, *137*, 4606 – 4609.
[39] Y. Hori, A. Murata, R. Takahashi, *J. Chem. Soc. Faraday Trans. 1* **1989**, *85*, 2309.

Received: May 12, 2016
Published online: July 5, 2016

